J Nanopart Res (2018) 20: 146
https://doi.org/10.1007/s11051-018-4246-y

PERSPECTIVES

Metal phosphonate coordination networks and frameworks as precursors of electrocatalysts for the hydrogen and oxygen evolution reactions

Rui Zhang · Sayed M. El-Refaei · Patrícia A. Russo · Nicola Pinna

Received: 13 February 2018 / Accepted: 2 May 2018 / Published online: 22 May 2018

Abstract The hydrogen evolution reaction (HER) and the oxygen evolution reaction (OER) play key roles in the conversion of energy derived from renewable energy sources into chemical energy. Efficient, robust, and inexpensive electrocatalysts are necessary for driving these reactions at high rates at low overpotentials and minimize energetic losses. Recently, electrocatalysts derived from hybrid metal phosphonate compounds have shown high activity for the HER or OER. We review here the utilization of metal phosphonate coordination networks and metal-organic frameworks as precursors/templates for transition-metal phosphides, phosphates, or oxyhydroxides generated in situ in alkaline solutions, and their electrocatalytic performance in HER or OER.

Keywords Metal phosphonate · Water splitting · Electrocatalysis

Introduction

The continuous growth of the world population and industrial sector will require the production of increasingly large amounts of energy over the next decades. Current energetic needs are mostly supplied by fossil fuels, such as petroleum, coal, and natural gas, but relying almost exclusively on fossil fuels to meet future energetic demands may have severe environmental consequences owing to their association with greenhouse gases emission and climate change (Cook et al. 2010; Lewis and Nocera 2006; Turner 2004). The development and improvement of technologies for sustainable production of energy based on renewable energy sources such as wind, sun light, or biomass is thus critical. However, intermittent renewable energy sources, such as the wind and sun, cannot provide the continuous and steady energy necessary for daily life and industrial production, which creates the need to develop technology to store the excess of energy harvested, for example, in the form of chemical energy in fuels like H_2 that can be later converted again to electrical energy using fuel cells (Turner 2004).

Water splitting, driven by renewable energy sources, is considered a promising method for the large-scale clean production of H_2, but there are still many challenges, from system efficiency to costs, hindering the widespread application of this process (Cook et al. 2010; Gray 2009; Kanan and Nocera 2008; Reier et al. 2017). Water splitting is an endothermic reaction with $\Delta G = 237.2$ kJ mol^{-1} and thermodynamic potential of 1.23 V at standard conditions. It comprises two half-cell reactions: the hydrogen evolution reaction (HER) at the cathode, and the oxygen evolution reaction (OER) at the anode. Both reactions require catalysts to drive them at high rates at low overpotentials, although the OER is

This article is part of the topical collection: 20th Anniversary Issue: From the editors

Nicola Pinna, Executive Editor, Mike Roco, Editor-in-Chief

R. Zhang · S. M. El-Refaei · P. A. Russo (✉) · N. Pinna (✉)
Institut für Chemie and IRIS Adlershof, Humboldt-Universität zu Berlin, Brook-Taylor-Str. 2, 12489 Berlin, Germany
e-mail: patricia.russo@hu-berlin.de
e-mail: nicola.pinna@hu-berlin.de

energetically more demanding, as it proceeds through a complex multistep mechanism involving the transfer of four electrons that decreases the efficiency of the entire process (Hunter et al. 2016; Suen et al. 2017; Zeng and Li 2015).

Platinum is the most active catalyst for the HER, whereas iridium and ruthenium oxides are the benchmark catalysts for the OER. However, a generalized commercialization of this technology requires catalysts that are simultaneously inexpensive, highly active, and stable, for competing with the scarce and expensive noble-metal-based catalysts. Consequently, in the past decades, considerable efforts have been devoted to the search for efficient HER and OER catalysts based on earth-abundant transition-metals (Han et al. 2016; Zeng and Li 2015).

Several different classes of transition-metal-based (Ni, Co, Fe, Cu, Mo, W) materials have been explored as HER electrocatalysts, including alloys (McKone et al. 2013), chalcogeneides (Cheng et al. 2014; Kong et al. 2013), carbides (Vrubel and Hu 2012), nitrides (Chen et al. 2012), and phosphides (Popczun et al. 2013; Xing et al. 2014). Transition-metal phosphides in particular have attracted much attention in recent years, as they are among the most active non-noble metal HER catalysts (Xiao et al. 2015). Their activity and long-term stability may be further improved by combination with carbon materials, which increases the electroconductivity of the catalyst, may lead to synergistic effects, and have a stabilizing effect (Bai et al. 2015; Pan et al. 2015).

Phosphides are also promising catalysts for the OER in alkaline conditions (Stern et al. 2015), as are phosphates (Kim et al. 2015), oxides (Trotochaud et al. 2012), and hydroxides (Gong et al. 2013) containing transition-metals such as Co, Ni, Fe, and Mn. In acidic media, on the contrary, no material based on earth-abundant transition-metals has been able to effectively compete with Ir and Ru oxides in promoting the oxidation of water (Reier et al. 2017). The lack of a complete understanding of the water oxidation mechanisms in acidic and basic solutions constitutes an additional barrier to the design of efficient OER catalysts (Dau et al. 2010; Suen et al. 2017). This makes it also desirable to have heterogeneous catalysts with well-defined structures containing well-known catalytic active sites distributions and structures in order to get a better understanding of the OER mechanisms, which, in turn, is useful for the development of more efficient catalytic materials. Therefore, the search for new electrocatalysts plays a key role in the development of energy conversion technologies.

In recent years, hybrid inorganic-organic materials, and in particular metal-organic frameworks (MOFs), have emerged as promising materials for energy storage and conversion applications (Downes and Marinescu 2017; Salunkhe et al. 2017). Research has been focused largely on the utilization of MOFs (many carboxylate-MOFs) as supports for catalytic active species, and templates/precursors for metal oxides and porous carbon structure (Morozan and Jaouen 2012; Salunkhe et al. 2017). Metal phosphonates are a group of hybrid inorganic-organic materials consisting of extended structures containing organophosphonate ligands coordinated to metal ions or clusters (Gagnon et al. 2012; Shimizu et al. 2009). This family of hybrid compounds includes dense layered coordination networks (CNs), porous coordination networks, MOFs, hybrids metal oxide/phosphonate, and polyoxometalates (POMs) (Gagnon et al. 2012; Mutin et al. 2015; Shimizu et al. 2009). Metal phosphonate CNs and MOFs have recently shown promise as materials for energy storage and conversion (Mei et al. 2017; Pramanik et al. 2015; Zhang et al. 2017a; Zhou et al. 2015). They have been utilized directly as the active material or as precursors/templates for electrocatalytic active materials such as phosphides (Zhang et al. 2017c), phosphates (Zhou et al. 2017), and hydroxides (Saha et al. 2017). Porous-doped carbon composites are also readily produced by carbonization of phosphonate compounds (Wang et al. 2018). Herein, we review the recent use of phosphonate CNs and MOFs as precursors/templates for HER and OER electrocatalysts. The application of some metal phosphonate materials in photocatalytic water splitting is also described.

Metal phosphonates

Metal phosphonates are hybrid inorganic-organic materials containing metals coordinately bonded to phosphonate ligands (Clearfield and Demandis 2011; Gagnon et al. 2012; Maeda 2004). Phosphonate ligands form strong bonds with a wide variety of metals, ranging from monovalent to hexavalent metals, and can coordinate through any of their three oxygen atoms and in any state of protonation, which can lead to many different structural arrangements, especially if additional ligands or functionalities are present (Gagnon et al. 2012; Goura

and Chandrasekhar 2015; Shimizu et al. 2009; Zhu et al. 2014). Although this makes the phosphonate chemistry versatile, it makes it complex and difficult to predict as well.

Owing to the strength of the metal phosphonate coordination bonds and P–C bonds, metal phosphonate CNs exhibit high thermal stability and chemical resistance compared with other coordination compounds (e.g., carboxylates), which allows them to withstand conditions that would destroy many other hybrid materials. The water solubility of metal phosphonates increases with the decrease of the metal valence: trivalent and tetravalent metal phosphonates have low solubilities, with tetravalent metal phosphonates being insoluble even in strongly acidic solutions; divalent metal phosphonates are soluble in slightly acidic media; and all monovalent metal phosphonates are soluble (Gagnon et al. 2012; Zhu et al. 2014; Zhu et al. 2015a). These properties together with the versatility of the metal phosphonate chemistry make them attractive materials for a wide variety of fields including catalysis, gas storage, sensing, energy storage, and energy conversion (Chen et al. 2017; Ma and Yuan 2011; Zhu et al. 2014; Zhu et al. 2015a).

Phosphonate CNs may have crystalline or amorphous structures. In general, the formation of crystalline solids becomes more difficult to achieve as the valence of the metal increases, owing to the lower solubility of the corresponding compounds that tend to precipitate rapidly as essentially amorphous materials (Gagnon et al. 2012). Furthermore, they can be synthesized with a variety of structures including 2D layered compounds (Clearfield 1998b), ordered mesostructured materials, and MOFs (Gagnon et al. 2012; Ma and Yuan 2011; Shimizu et al. 2009). These characteristics depend mainly not only on the metal and phosphonate ligands, but also on the synthesis conditions such as solvent, reaction time, or presence of surfactants on the reaction mixture.

Many metals react with phosphonic acids to form two-dimensional (2D) layered structures. These structures consist of inorganic layers formed by metal ions or clusters bonded to the oxygen atoms of the bridging phosphonate groups, which are separated by layers of the organic moieties of the ligand molecules (Clearfield 1998b). The porosity of layered structures can be increased by replacing some of the phosphonate ligands with small groups such as phosphate, phosphite or a smaller monophosphonate molecule (Alberti et al. 1998; Clearfield 1998a; Dines et al. 1983; Zhu et al. 2014). These small groups act as "spacers" and create voids in the interlayer region. Porosity can also be generated in phosphonate coordination networks with the addition to the reaction mixtures of small molecules (e.g., β-cyclodextrin) or polymers (Ma and Yuan 2010; Polarz et al. 2001). Soft-templating strategies involving cationic (alkyltrimethylammonium cations) or non-ionic surfactants (triblock copolymers) are used for fabricating mesoporous phosphonate networks (El Haskouri et al. 2004; Ma et al. 2010; Ma and Yuan 2011; Zhu et al. 2015a). These materials may be either crystalline or amorphous. Many phosphonate-based MOFs have been reported in the literature, which were synthesized using ligands such as arylphosphonates, piperazinylphosphonates, alkylbisphosphonates, or methylphosphonate (Gagnon et al. 2012; Poojary et al. 1995; Shimizu et al. 2009; Wharmby et al. 2010; Zhu et al. 2000). Phosphonate ligands having a second chelating functional group can also be used to produce MOFs (Shimizu et al. 2009). Typical moieties on the phosphonate ligand include carboxylic, hydroxyl, pyridine, imino, and sulfonic acid groups. The synthesis of metal phosphonate compounds has been reviewed extensively in several publications (Clearfield and Demandis 2011; Gagnon et al. 2012; Maeda 2004; Shimizu et al. 2009; Zhu et al. 2014, 2015a

Hydrogen evolution and oxygen evolution reactions

Water splitting is the splitting of water into gaseous O_2 and gaseous H_2 (Eq. 1). In combination with renewable energy sources, it is a promising sustainable method for the large-scale production of hydrogen, which is a fuel for environmentally friendly energy conversion technologies such as fuel cells (Cook et al. 2010; Lewis and Nocera 2006; Turner 2004).

$$2H_2O \rightarrow 2H_2(g) + O_2(g) \quad (1)$$

Water splitting comprises two half-reactions: the cathodic half-reaction is the hydrogen evolution reaction (HER; Eqs. 2 and 3) and the anodic half-reaction is the oxygen evolution reaction (OER; Eqs. 4 and 5).

HER:

$$2H^{+}_{(aq)} + 2e^{-} \rightarrow H_{2(g)} \quad \text{(in acidic media)} \tag{2}$$

$$2H_2O_{(l)} + 2e^{-} \rightarrow H_{2(g)} + 2OH^{-}_{(aq)} \quad \text{(in alkaline media)} \tag{3}$$

OER:

$$2H_2O_{(l)} \rightarrow O_{2(g)} + 4H^{+}_{(aq)} + 4e^{-} \quad \text{(in acidic media)} \tag{4}$$

$$4OH^{-}_{(aq)} \rightarrow O_{2(g)} + 2H_2O_{(l)} + 4e^{-} \quad \text{(in alkaline media)} \tag{5}$$

These electrochemical reactions do not proceed at the equilibrium potential and only start when sufficiently large overpotentials are applied. Electrocatalysts are necessary to decrease the overpotential and increase the energetic efficiency of the process.

The hydrogen evolution reaction involves the transfer of two electrons to produce one H_2 molecule, and it is generally accepted that it proceeds through two reaction steps (Zeng and Li 2015). It is initiated by a discharge reaction, also known as the Volmer reaction ($H^+ + e^- \rightarrow H_{ad}$, in acidic media). Subsequently, the reaction may proceed through the Heyrovský reaction, which involves the combination of an adsorbed hydrogen atom with a proton from the solution to form H_2 [$H_{ad} + H^{+}_{(aq)} + e^- \rightarrow H_2(g)$], or through the Tafel reaction, which consists in the combination of two adsorbed hydrogen atoms to form H_2 [$H_{ad} + H_{ad} \rightarrow H_2(g)$]. The Tafel slopes of the HER are 118 mV dec^{-1}, 39 mV dec^{-1} and 30 mV dec^{-1} if the rate-determining step is the Volmer, Heyrovský or Tafel reaction, respectively.

The OER is a complex multistep reaction involving the transfer of four electrons to form one O_2 molecule, making it kinetically sluggish and thus decreasing the efficiency of the overall water splitting process. The complexity of this stepwise reaction makes water oxidation difficult to achieve without the application of a significant overpotential.

The OER mechanisms in both acidic and alkaline electrolytes are not completely understood yet, although several mechanisms have been proposed based on experimental observations and computational simulations (Dau et al. 2010; Suen et al. 2017). Most of the proposed mechanisms involve the formation of high-energy surface intermediates (such as MO, MOH, or MOOH, where M is a metal active site), and it is generally accepted that the bonding in the reaction intermediates plays a key role in the electrocatalytic activity of the catalyst.

Various parameters are used for evaluating the performance of HER and OER electrocatalysts, namely the overpotential at a given current density, the Tafel slope, the turnover frequency (TOF), or the Faradaic efficiency (McCrory et al. 2015; Stevens et al. 2017). One of the main parameters used is the overpotential necessary to achieve a current density per geometric area of 10 mA cm^{-2}. This is approximately the current density at the anode of a solar water-splitting device under 1 sun illumination operating at 10% solar-to-fuels efficiency (McCrory et al. 2015). The Tafel slope is a kinetic parameter that reflects the increment in overpotential necessary to cause a tenfold increase of the current density, and it is another important parameter utilized for comparing electrocatalysts (Zeng and Li 2015). The smaller the Tafel slope the more efficient is the catalyst at enhancing the reaction kinetics. In addition, the Tafel slope may provide insights into the mechanisms of the reactions. The TOF, defined as the number of catalytic cycles per unit of time, provides information about the intrinsic activity of the catalysts (Stevens et al. 2017). The Faradaic efficiency is the ratio of the amount of product generated by the electrochemical reaction to the theoretical amount according to Faraday's law. Ideal catalysts should have small overpotentials at j = 10 mA cm^{-2}, low Tafel slopes, high TOF values, and Faradaic efficiencies close to unity.

Metal phosphonates as precursors for HER electrocatalysts

Transition-metal phosphonates have been recently explored as precursors for the synthesis of metal phosphide materials that efficiently catalyze the HER. The electrocatalysts reviewed here are summarized in Table 1.

Zhu et al. (Zhu et al. 2015b) fabricated a composite HER electrocatalyst consisting of a porous N,P-codoped carbon network decorated with cobalt phosphide nanocrystals from a cobalt phosphonate precursor. The metal phosphonate was synthesized from $CoCl_2.6H_2O$, 1-hydroxyethylidene-1,1-diphosphonic acid, and melamine. Calcination of the hybrid at 900 °C under N_2 lead to the one-step formation of CoP nanoparticles of ca. 2–

Table 1 Summary of the HER and OER electrocatalysts based or derived from metal phosphonates reviewed here

Metal phosphonate precursor	Catalyst	Synthesis conditions	Electrolyte	Substrate	Loading (mg cm^{-2})	η at 10 mA cm^{-2} (mV)	Tafel slope (mV dec^{-1})	Ref.
HER								
Co(II) 1-hydroxyethylidene-1, 1-diphosphonate/melanine	CoP@NPC CoP NCs on N, P-codoped carbon	Calcination at 900 °C under N_2	0.5 M H_2SO_4	GC	0.26	123	69	(Zhu et al. 2015b)
Cu(III) hydroxyethylidene-1, 1-diphosphonate/pyrazine	Cu_3P@NPPC Cu_3P NPs coated with N, P-codoped carbon	Calcination at 650 °C under N_2; phosphidation with NaH_2PO_2 at 250 °C under N_2	0.5 M H_2SO_4	GC	0.29	89	76	(Wang et al. 2017)
$Ni(II)O_3PC_6H_5.H_2O$/ $Ni(II)O_3PCH_3.H_2O$	Ni_2P NPs coated with carbon	Calcination at 550 °C under H_2(5%)Ar	0.5 M H_2SO_4	GC	0.42	87	64	(Zhang et al. 2017c)
$Ni(II)O_3PC_6H_5.H_2O$	$Ni_{12}P_5/Ni_2P$ NPs coated with carbon	Calcination at 500 °C under H_2(5%)Ar	0.5 M H_2SO_4	GC	0.42	132	85	(Zhang et al. 2017c)
OER								
$CoO_3PCH_3.H_2O$	$CoO_3PCH_3.H_2O$	–	Water-saturated [BMIM][PF6]	GC	0.11	~1.45*	–	(Liu et al. 2013)
$CoO_3PC_2H_5.H_2O$	$CoO_3PC_2H_5.H_2O$	–	Water-saturated [BMIM][PF6]	GC	0.11	~1.45*	–	(Liu et al. 2013)
Co(*n*-$O_3PC_4H_9.H_2O$)	Co(*n*-$O_3PC_4H_9.H_2O$)	–	Water-saturated [BMIM][PF6]	GC	0.11	~1.50*	–	(Liu et al. 2013)
$CoO_3PC_6H_5.H_2O$	$CoO_3PC_6H_5.H_2O$	–	Water-saturated [BMIM][PF6]	GC	0.11	~1.55*	–	(Liu et al. 2013)
Co(II) nitrilotris(methylene) triphosphonate	CoOOH	In situ formation	1 M NaOH	GC	0.065	380	67	(Saha et al. 2017)
$Ni_{0.84}Fe_{0.16}O_3PC_6H_5.H_2O$	$Ni_{0.84}Fe_{0.16}$ LDH	In situ formation	1 M KOH	GC	0.42	240	40	(Zhang et al. 2017b)
$Co_3(O_3PCH_2NC_4H_7CO_2)_2.4H_2O$	$Co_3(O_3PCH_2NC_4H_7CO_2)_2.4H_2O$	–	0.1 M phosphate buffer (pH = 7)	GC	0.25	484§	83	Zhou et al. 2015)
Co(II) (4-phosphonomethylamino-methylbenzoic acid)	$Co_2P_2O_7/Co_3(PO_4)_2$ (1:2) NPs surrounded by N-doped carbon	Calcination at 800 °C under N_2	1 M KOH	GC	0.41	260	64	(Zhou et al. 2017)

* E vs Fc/Fc^+ (V) at a current of 50 μA; § overpotential at a current density of 1 mA cm^{-2}

5 nm uniformly loaded on N,P-doped carbon (CoP@NPC), without the need of additional phosphorous sources or phosphorization steps. The CoP@NPC material has a high surface area of 867 $m^2\ g^{-1}$ due to the highly porous carbon network derived from the organic ligands. Porosity and high surface area are advantageous properties for electrocatalysis, as they normally result in increased electrochemical active surface areas of the catalysts and access of the electrolytes to a higher number of actives sites in comparison with low surface area materials. The HER electrocatalytic activity of the composite deposited on a glassy carbon (GC) electrode was measured in 0.5 M H_2SO_4. CoP@NPC generated current densities of 10 and 20 mA cm^{-2} at overpotentials of 123 and 156 mV, respectively, and outperformed a catalyst prepared by post-synthesis combination of CoP and NPC. The activity of CoP@NPC was attributed to the increase of the electroconductivity caused by the doped carbon that facilitates the charge-transfer, the strong coupling between the NPC and CoP, and to the porous structure that provides accessible active sites and facilitates the mass transfer.

Very recently, a similar strategy was reported for preparing Cu_3P nanoparticles (NPs) coated with a N,P-codoped carbon network (Cu_3P@NPPC) (Wang et al. 2017). First, a copper MOF was synthesized by refluxing $Cu(NO_3)_3.3H_2O$, 1-hydroxyethylidene-1,1-diphosphonic acid, and pyrazine in water at 140 °C for 5 h. The Cu-NPMOF was then calcined 4 h under N_2 at 600, 650, or 700 °C, followed by phosphidation with NaH_2PO_2 under N_2 atmosphere at 250 °C to generate the Cu_3P@NPPC materials (Fig. 1). The composites were drop-casted onto a GC electrode and tested in 0.5 M H_2SO_4 solution. The material prepared by calcination at 650 °C had the highest surface area (1004 $m^2\ g^{-1}$) and exhibited the best HER performance, requiring only overpotentials of 89, 117, and 207 mV to reach current densities of 10, 20 and 80 mA cm^{-2} (Fig. 2), and comparing favorably with other Cu phosphide catalysts reported in the literature. The high HER activity of Cu_3P@NPPC was ascribed to the combination of i) high surface area that allows a high number of active sites available for reaction; ii) the synergistic effects of Cu_3P NPs and N,P-codoped carbon; iii) and the enhanced electroconductivity due to presence of the carbon. Additionally, the carbon provides physical and chemical protection to the Cu_3P NPs, as the composite electrocatalyst exhibited high stability, showing a

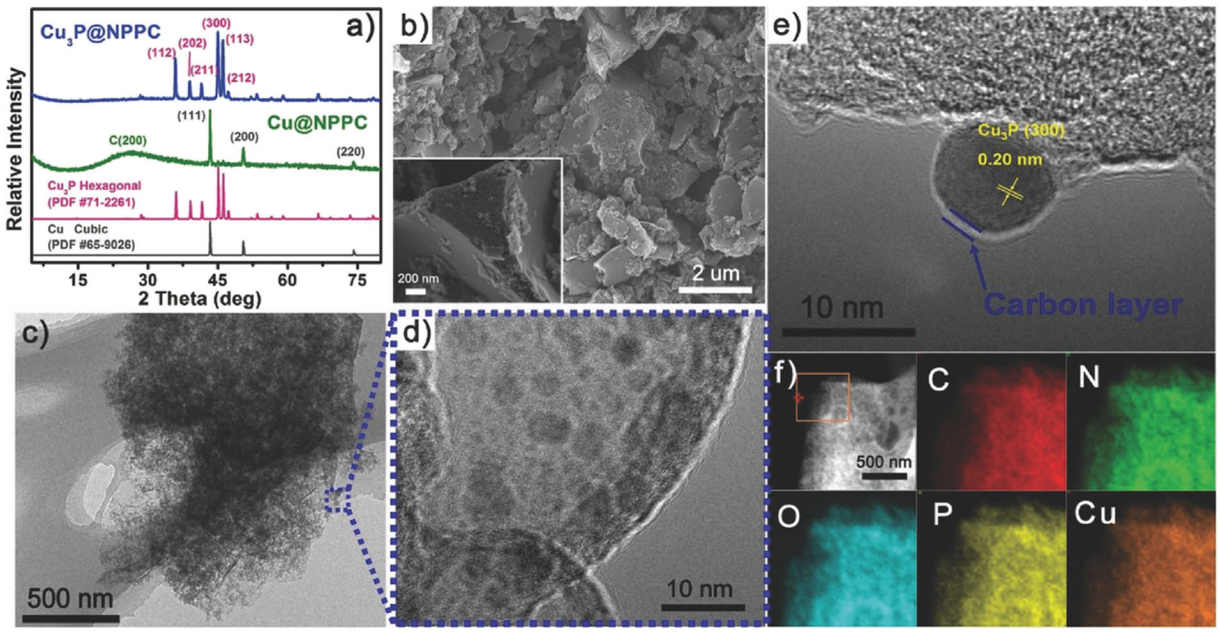

Fig. 1 **a** Powder XRD patterns of Cu_3P@NPPC and of the calcined material prior to phosphidation (Cu@NPPC). **b** SEM images of Cu_3P@NPPC. **c**–**e** TEM and HRTEM images of Cu_3P@NPPC (the bright contrast which is indicated as a carbon coating in (**e**) is likely to be an artifact caused by non-ideal focusing conditions). **f** Elemental mapping images of Cu_3P@NPPC showing the uniform presence of C, N, O, P, and Cu. Reproduced with permission (Wang et al. 2017). Copyright 2017, Wiley-VCH

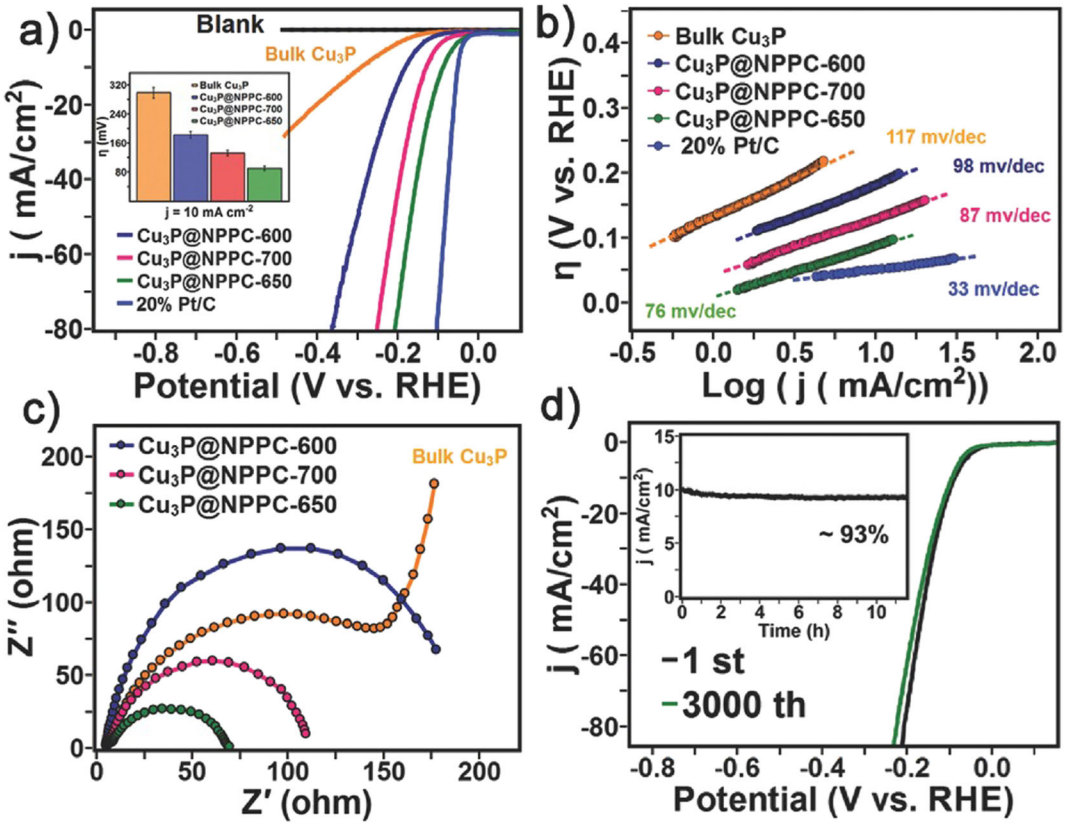

Fig. 2 **a** LSV curves of various samples for HER in 0.5 m H_2SO_4 (inset: the error bar of HER activities for Cu_3P@NPPC catalysts) and **b** the corresponding Tafel curves. **c** Nyquist plots of the Cu_3P@NPPC and bulk Cu_3P samples at − 0.2 V over the frequency range from 100,000 to 1 Hz. **d** HER stability tests of the Cu_3P@NPPC-650 catalyst. Reproduced with permission (Wang et al. 2017). Copyright 2017, Wiley-VCH

current density loss of just 7% during a chronoamperometry measurement of 11 h, and no detectable changes in composition and structure.

Zhang et al. synthesized 2D layered $NiO_3PC_6H_5.H_2O$ and $NiO_3PCH_3.H_2O$ compounds and used them as single-source precursors for fabricating nickel phosphide nanoparticles covered with thin carbon films (Zhang et al. 2017c). Calcination of the hybrid materials under H_2(5%)/Ar atmosphere at temperatures of 450, 500, and 550–700 °C, produced respectively $Ni_{12}P_5$, mixed $Ni_{12}P_5$/Ni_2P, and Ni_2P NPs with sizes of 15–45 nm and coated with carbon (Fig. 3). Nickel phosphide phases were also produced by calcination under pure argon. Thermogravimetric analysis coupled with mass spectrometry revealed the formation of H_2, H_2O, P_2 and C_6H_5 during the calcination of the metal phosphonate under Ar. It was proposed that the H_2 produced in situ reacted with the PO_3 groups of the material to form H_2O and P_2, and the latter subsequently reacted with the metal to generate the metal phosphide. The Ni_2P NPs, deposited on a GC electrode, efficiently catalyzed the HER in 0.5 M H_2SO_4 solution, with an overpotential at j = 10 mA cm^{-2} of 87 mV and Tafel slope of 64 mV dec^{-1} (Fig. 4). Potential cycling and long-term electrolysis measurements of the Ni_2P electrocatalyst showed small losses of activity after 1000 cycles or 11 h of electrolysis at j = 10 mA cm^{-2} (Fig. 4), compared to those reported for other Ni_2P nanostructured catalysts, owing to the protective effect of the thin carbon shell surrounding the NPs that partly hinders the dissolution of the Ni phosphide in the acidic electrolyte.

Metal phosphonates as precursors for OER electrocatalysts

In 2011, Shevchenko et al. (Shevchenko et al. 2011) observed the formation in situ of a cobalt-based water

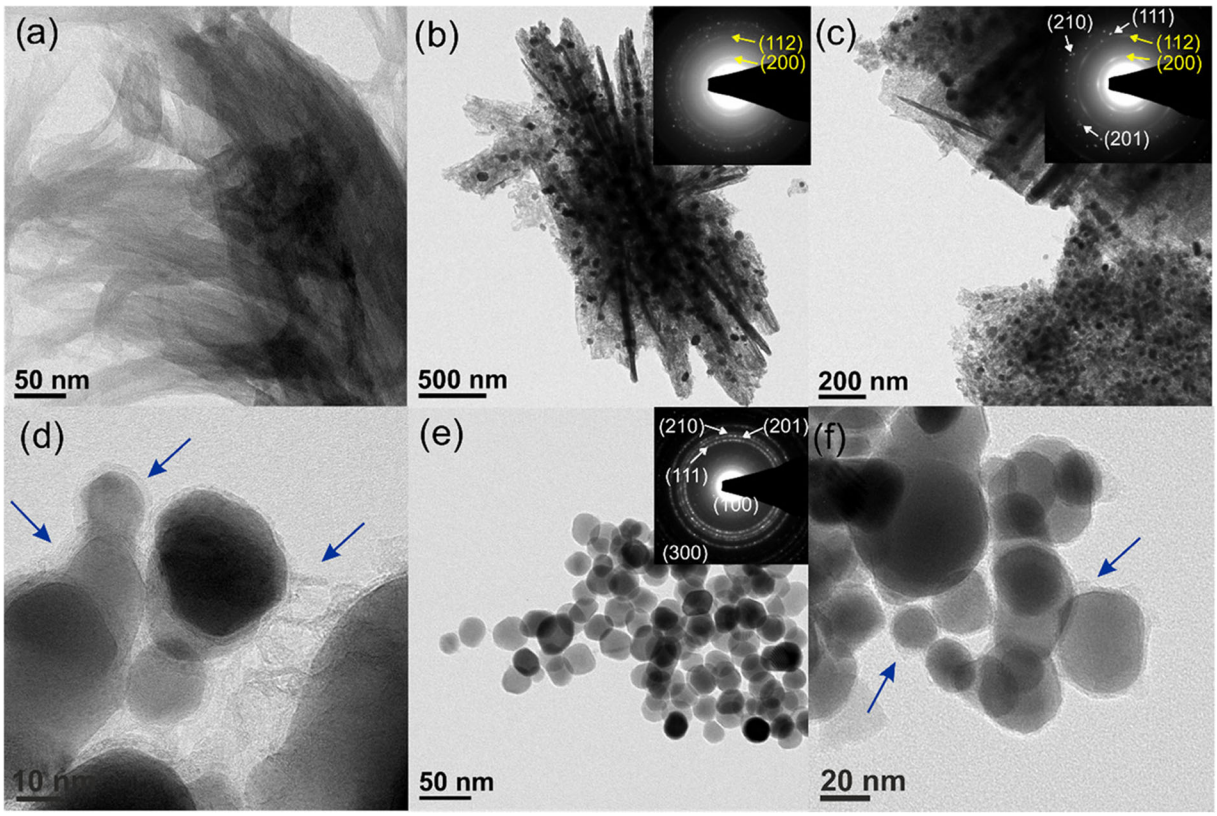

Fig. 3 TEM images of **a** nickel phenylphosphonate and **b** $Ni_{12}P_5$-Ph, **c**, **d** $Ni_{12}P_5$-Ni_2P-Ph, and **e**, **f** Ni_2P-Ph synthesized by thermal treatment of nickel phenylphosphonate under H_2(5%)/Ar at 450, 500, and 550 °C, respectively. The insets in (**b**), (**c**), and (**e**) show the SAED patterns (white, Ni_2P; yellow, $Ni_{12}P_5$). The arrows indicate the carbonaceous shell around the NPs. Reproduced with permission (Zhang et al. 2017c). Copyright 2017, American Chemical Society

oxidation catalyst from a Co(II)-methylened iphosphonate (M2P) precursor in phosphate buffer solution at pH = 7 under visible light illumination. The cobalt material particles (with a radius of 10–60 nm) catalyzed the water splitting driven by visible light, using $[Ru(bpy)_3]^{2+}$ (bpy = 2,2′-bipyridine) as a photosensitizer and persulfate ($S_2O_8^{2-}$) as an electron acceptor. The nanoparticles could catalyze the production of ~ 20 O_2 molecules per cobalt atom at a rate of ~ 0.2 mol O_2 s^{-1} (mol Co)$^{-1}$. No electrochemical tests were performed on this catalyst. The structure of the material formed in situ was subsequently determined in a later study by X-ray absorption spectroscopy (XAS) measurements at the Co K-edge, Co L-edge, and O K-edge (Risch et al. 2012). The XAS Co K-edge data revealed that the active catalyst is a cobalt (III) oxide core with a structure similar to that of electrodeposited cobalt catalysts. In those structures, CoO_6 octahedra form a layered cobalt oxide through edge-sharing (di-μ-oxo bridging). XAS measurements at the Co L-edge and O K-edge provided information regarding the binding of the methylenediphosphonate ligand. The data suggested that the M2P ligand is coordinated to the Co ions at the edge of the cobalt oxide nanoparticles obtained by light-oxidation of the Co/M2P precursor. The phosphonate ligands could be used to link a photosensitizer directly to the active cobalt oxide catalyst and utilize the solar energy directly for fuel production.

Liu et al. (2013) first reported the OER activity of a series of layered Co(II) phosphonates in 2013 (Table 1). Four isostructural compounds were prepared by hydrothermal reaction of Co^{2+} ions with methylphosphonic acid, ethylphosphonic acid, *n*-butylphosphonic acid or phenylphosphonic acid. The Co phosphonates were deposited onto GC electrodes and their OER activity was measured in 0.1 M phosphate buffer (pH = 7). All the catalysts showed similar OER activity in phosphate buffer, likely due to their conversion into a CoO_x catalyst caused by their instability under the measurement conditions, although no characterization of the materials after

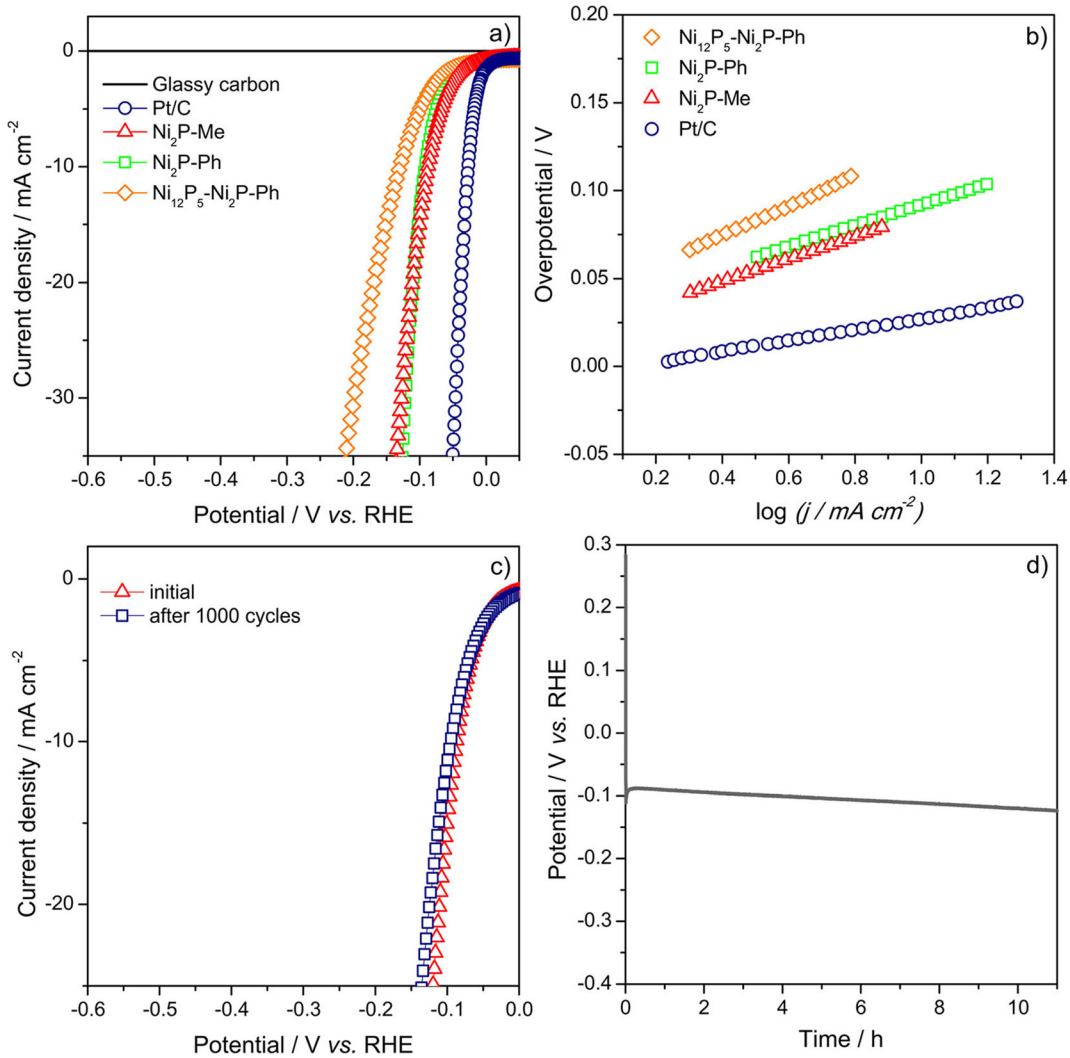

Fig. 4 **a** Polarization curves and **b** Tafel plots of $Ni_{12}P_5$-Ni_2P-Ph, Ni_2P-Ph, Ni_2P-Me, and Pt/C in 0.5 M H_2SO_4 (scan rate, 10 mV s^{-1}; 2000 rpm). **c** Polarization curves of the Ni_2P-Me NPs measured before and after 1000 CV cycles (between − 0.2 and 0.2 V vs RHE; scan rate: 100 mV s^{-1}) in 0.5 M H_2SO_4. **d** Variation of the overpotential as a function of time for Ni_2P-Me, measured at a constant cathodic current density of 10 mA cm^{-2}. Reproduced with permission (Zhang et al. 2017c). Copyright 2017, American Chemical Society

electrocatalysis was performed. The OER performance of the four phosphonates was subsequently tested in a water-saturated ionic liquid [BMIM][PF6], which was expected to provide a more stable environment for the catalysts. Differences in the catalytic activity were observed for the Co phosphonates with different ligands. The activity decreased in the sequence methyl>ethyl>n-butyl>phenyl, which could be a consequence of the different intrinsic activity of the catalysts, and/or the different rates of their conversion into CoO_x catalysts (Table 1).

The effect of the porosity and surface area of cobalt phosphonates on the OER was recently investigated (Saha et al. 2017). Cobalt phosphonates with different amounts of narrow micro/mesopores were synthesized from $CoCl_2.6H_2O$ and nitrilotris(methylene)triphosphonic acid (NMPA) using triblock copolymer F127 as surfactant and polyvinyl alcohol (PVA) as co-surfactant. After extraction of the surfactants, amorphous Co phosphonates consisting of agglomerated spheres were obtained. The spheres contained hollow cores with size 20–60 nm and narrow micro/mesopores (1.5–5 nm) on the walls. The amount of narrow micro/mesoporosity and the surface area increased from 61 to 76 m^2 g^{-1} with the increase of the PVA wt.% in the

reaction mixture from 0 to 15, respectively. The electrocatalytic OER activity of the hybrid materials deposited on a GC substrate was measured in 1 m NaOH. The overpotential at a current density of 10 mA cm^{-2} decreased from 446 to 380 mV, and the Tafel slope decreased from 79 to 67 mV dec^{-1} with increasing the amount of micro/mesoporosity and the surface area. The trend resulted from the increase in the amount of catalytic active sites contacting with the electrolyte as the surface area of the catalyst increased. Characterization of the material after 10 min of electrocatalysis revealed that the Co phosphonates acted as precatalysts for cobalt oxyhydroxides formed in situ in the alkaline solution. Interestingly, despite the phosphonate ligands being completely leached from the electrode film, the morphology of the initial phosphonate material was maintained on the oxyhydroxide, which lead to the different activities observed. Therefore, the phosphonate acted also as an in situ template for the morphology of the catalyst.

Layered mixed NiFe-phenylphosphonates were used as in situ precursors for NiFe hydroxide OER electrocatalysts in basic solution (Zhang et al. 2017b). The metal phosphonates act as in situ templates of small (5–25 nm) and very thin (3 to 10 nm) NiFe hydroxide nanosheets (Fig. 5). The Ni/Fe ratio could be easily controlled in the phosphonate precatalyst and an optimum catalytic activity was achieved for a Fe atomic

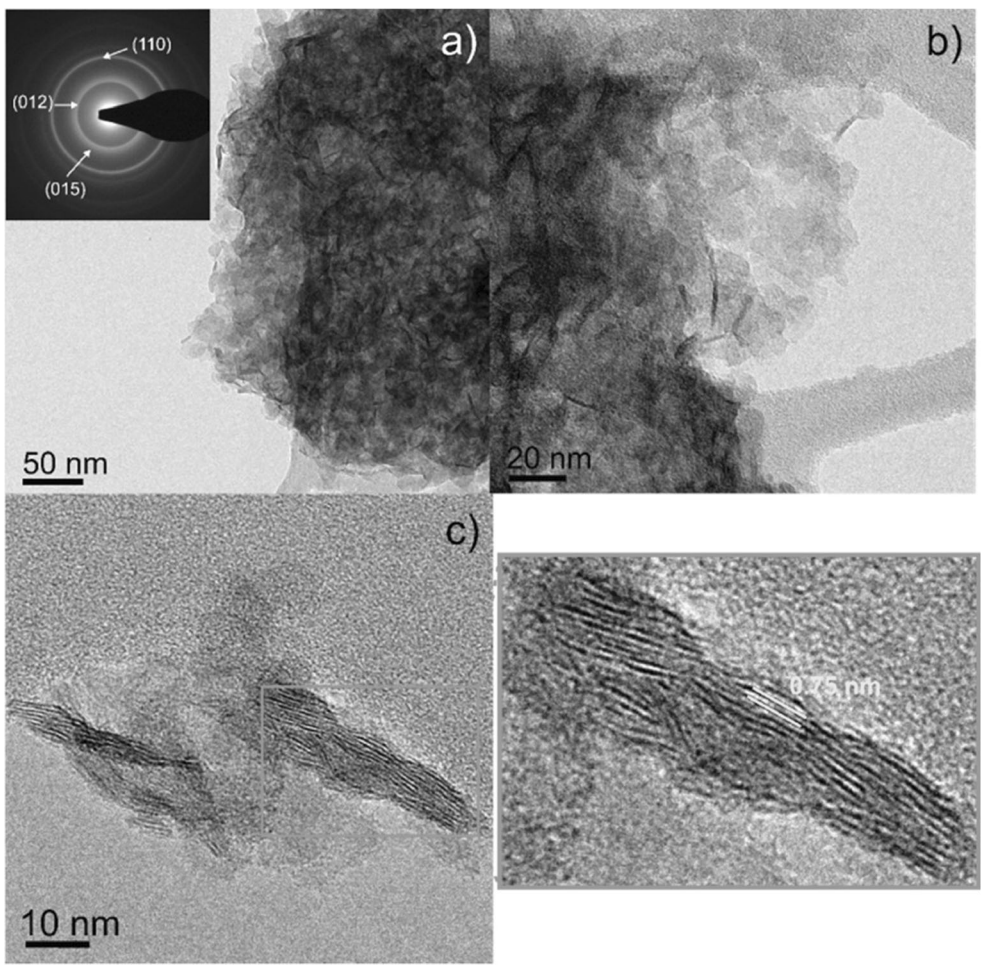

Fig. 5 TEM images of the NiFe16 catalyst after 50 potential cycles (NiFe16-50CV) in 1 M KOH in the potential window of 0–0.7 V versus Ag/AgCl (the interlayer distance in the hydroxide is 0.75 nm). The SAED pattern (inset in (a)) shows diffraction rings indexed to the (012), (015), and (110) of the hydroxide. Reproduced with permission (Zhang et al. 2017b). Copyright 2017, Wiley-VCH

content of 16%. This material exhibited an overpotential at j = 10 mA cm^{-2} of 240 mV, and a Tafel slope of 40 mV dec^{-1}, outperforming NiFe oxide and NiFe hydroxide catalysts used as reference (Fig. 6). In addition, the catalyst formed in situ has high long-term stability, being able to performing electrolysis at 10 mA cm^{-2} for 160 h continuous with little change in the overpotential (Fig. 6). The NiFe phenylphosphonates are composed of inorganic layers of distorted corner-shared NiO_6 and FeO_6 octahedra, which are transformed into edge-shared octahedra in the hydroxide. XAS measurements suggested that the local structure of the metals is not able to relax completely during the conversion of the phosphonate into the hydroxide, and consequently the geometry of the metal sites in the hydroxide deviates from the regular octahedral geometry. In other words, the metal phosphonate seems to act as a template for the local structure of the metal sites (Fig. 7). The efficient performance of the catalyst was attributed to the synergy between Ni and Fe, and to the presence of distorted metal sites that further promote water oxidation.

Zhou et al. (Zhou et al. 2015) exploited the versatile phosphonate chemistry to synthesize a cobalt-based water oxidation catalyst with structural features mimicking those of the Mn_4CaO_5 cluster in photosystem II, which is responsible for biocatalytic water oxidation. This cluster adopts a distorted coordination chemistry with octahedra linked through di-μ-oxo (edge-shared) or

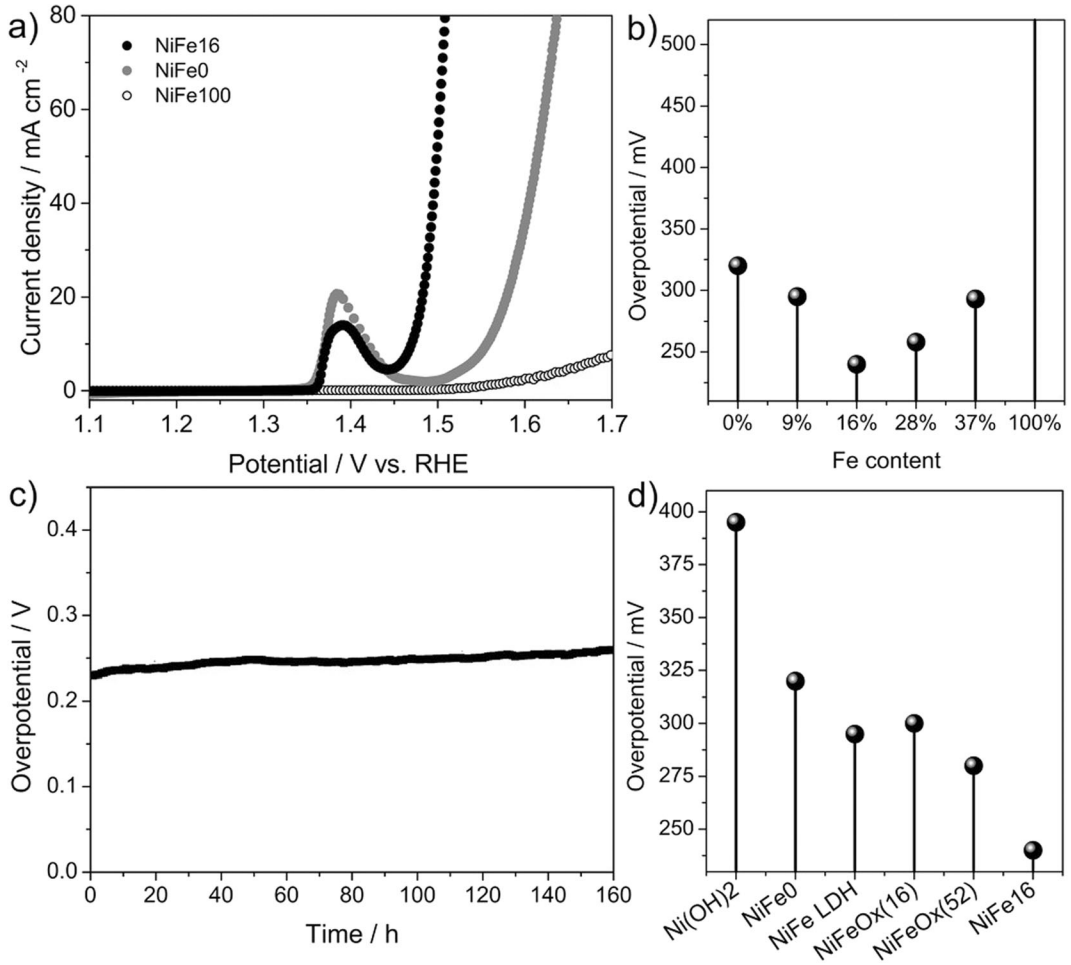

Fig. 6 **a** LSV curves of NiFe0, NiFe16, and NiFe100 measured in 1 M KOH (scan rate: 10 mV s^{-1}); **b** comparison of the overpotentials at j_{geom} = 10 mA cm^{-2} of the NiFe*x* catalysts as a function of the Fe at%; **c** variation of the overpotential at j_{geom} = 10 mA cm^{-2} with time for NiFe16; **d** comparison of the overpotentials at j_{geom} = 10 mA cm^{-2} of NiFe0, NiFe16, $Ni(OH)_2$, NiFe-LDH, NiFeOx(16), and NiFeOx(52) catalysts. Reproduced with permission (Zhang et al. 2017b). Copyright 2017, Wiley-VCH

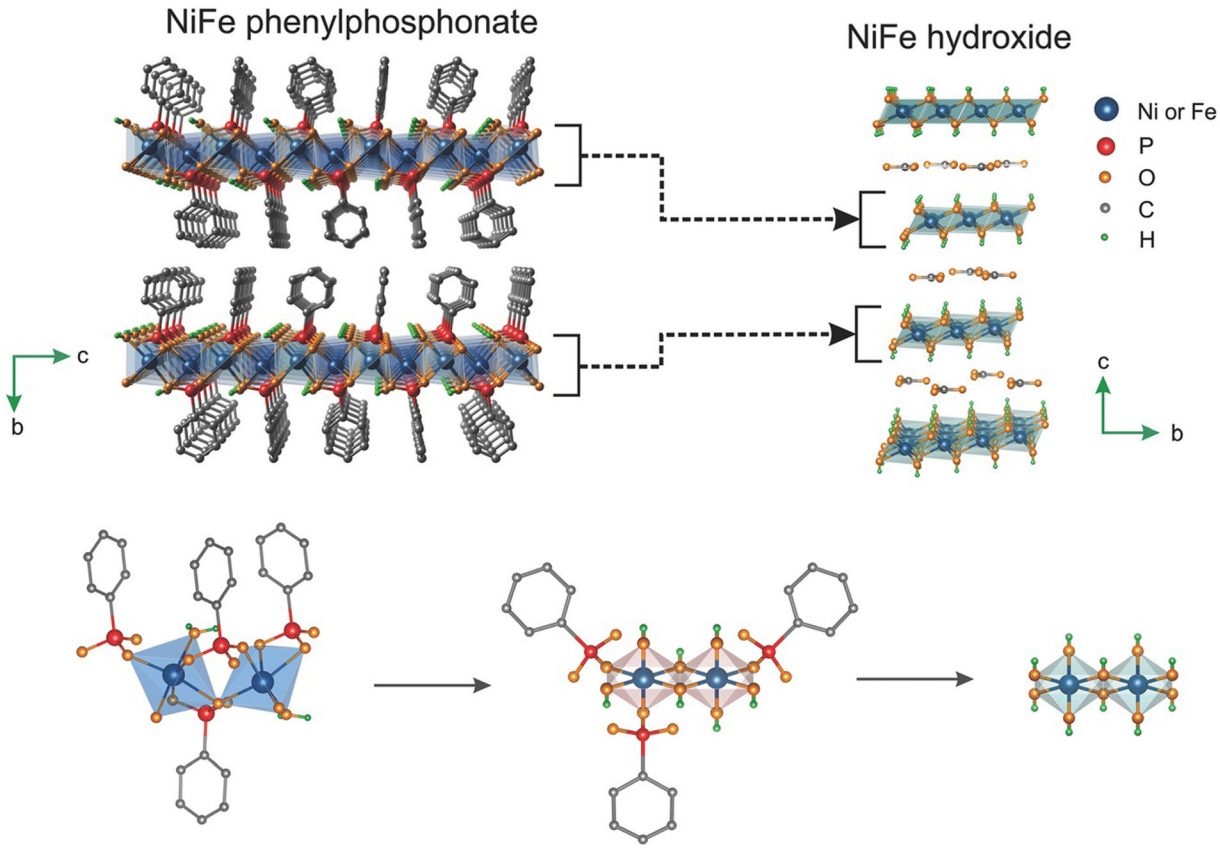

Fig. 7 Transformation of the NiFe-phenylphosphonate catalyst into the hydroxide. Reproduced with permission (Zhang et al. 2017b). Copyright 2017, Wiley-VCH

mono-μ-oxo (corner-shared) bridges. The layered cobalt phosphonate, $Co_3(O_3PCH_2–NC_4H_7–CO_2)_2.4H_2O$ (1) contains edge-sharing (di-μ-oxo bridging) and corner sharing (mono-μ-oxo bridging) CoO_6 octahedra. The asymmetric unit of this compound contains three Co(II) ions octahedrically coordinated. Both Co1 (CoO_5N) and Co2 (CoO_5N) are octahedrally coordinated by three phosphonate oxygen atoms, one carboxylate oxygen atom from three organic ligands, one nitrogen atom from one organic ligand as well as one aqua ligand. Co3 (CoO_6) is octahedrally coordinated by three phosphonate oxygen atoms and one carboxylate oxygen atom from four organic ligands as well as two aqua ligands (Fig. 8). Pairs of di-μ-oxo bridged CoO_6 and CoO_5N cobalt octahedra are linked via corner-sharing oxygen atom (O5) into Co–O chains consisting of a cubane-like Co_4O_5 unit along the c-axis. All the cobalt atoms have a distorted octahedral coordination geometry.

Three additional layered cobalt phosphonates were investigated for comparison: (i) $Co_3(O_3PCH_2–NC_4H_7–CO_2)_2.5H_2O$ (2) displays similar structural motifs as (1), although slightly less distorted Co coordination geometry; (ii) $Co_3(O_2C\text{-}CH_2CH_2\text{-}PO_3)_2.6H_2O$ (3) contains di-μ-oxo bridging CoO_6 octahedra; (iii) and compound $Co(O_3PC_6H_5).H_2O$ (4) contains corner-shared CoO_6 octahedra (Fig. 9).

The photocatalytic water oxidation activity of the phosphonates under visible light illumination was evaluated in sodium borate solution (pH = 9), using $[Ru(bpy)_3]Cl_2$ as the photosensitizer, and $Na_2S_2O_8$ as the sacrificial oxidant. The O_2 evolution rate and O_2 yield increased in the sequence 1 ~ 2 > 3 > 4. Compound (1) also performed better than a Co_3O_4 catalyst. Characterization of the material after the photocatalytic reaction by XRD, IR, XPS and HRTEM indicated no changes in the phosphonate structure. The electrochemical OER performance of the phosphonates on a GC substrate was evaluated by CV and LSV in 0.1 M phosphate buffer (pH 7) (Table 1). The overpotential of the phosphonate compounds follow the same trend observed for the photocatalytic water oxidation.

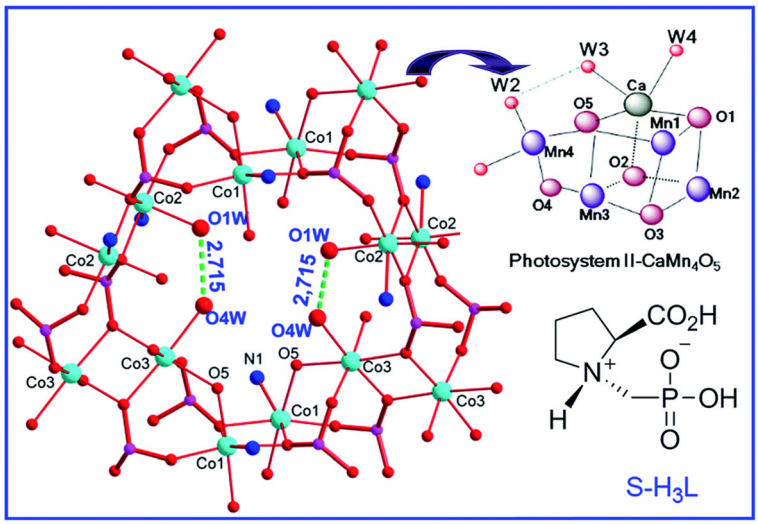

Fig. 8 Ball and stick view highlighting the connectivity of the pairs of cobalt octahedra for 1. Co,O, P, andN are shown as cyan, red, magenta, blue, respectively (where, S-H_3L = $H_2O_3PCH_2$–NC_4H_7–CO_2H). Reproduced with permission (Zhou et al. 2015). Copyright 2015, Royal Society of Chemistry

Correlation of the catalytic performances with the well-defined crystal structures of the phosphonates suggests that the presence of extensive di-μ-oxo bridged and mono-μ-bridged cobalt octahedral leads to higher activity, and that the compound with the more distorted Co coordination environment displays higher catalytic activity.

Cobalt phosphate OER electrocatalysts were produced by calcination of a layered cobalt phosphonate (Zhou et al. 2017). The precursor was prepared by hydrothermal reaction of $Co(NO_3)_2.6H_2O$ with (4-[(Phosphonomethylamino)-methyl]benzoic acid) at 140 °C for 72 h, and subsequently calcined under N_2 at 400 °C for 2 h followed by 2 h at 800 °C. The resultant material (H3LCoCN800) consists of ca. 5 nm Co phosphate NPs surrounded by N-doped carbon (Fig. 10). EXAFS analysis revealed that the catalyst contains monoclinic cobalt diphosphate $Co_2P_2O_7$ (ca. 31 wt.%) and $Co_3(PO_4)_2$ (ca. 64 wt%) in a ratio 1:2. This catalyst generated a current density of 10 mA cm^{-2} at an overpotential of 260 mV on a GC substrate in 1 M KOH, and was more active than a similar catalyst containing a higher percentage of $Co_3(PO_4)_2$ (ca. 86 wt%) that was prepared by calcination at 700 °C (Fig. 11). The higher activity was associated with a higher content of $Co_2P_2O_7$, which was correlated with the structural characteristics of the $Co_2P_2O_7$ and $Co_3(PO_4)_2$. The cobalt atoms in $Co_2P_2O_7$ display a more distorted coordination

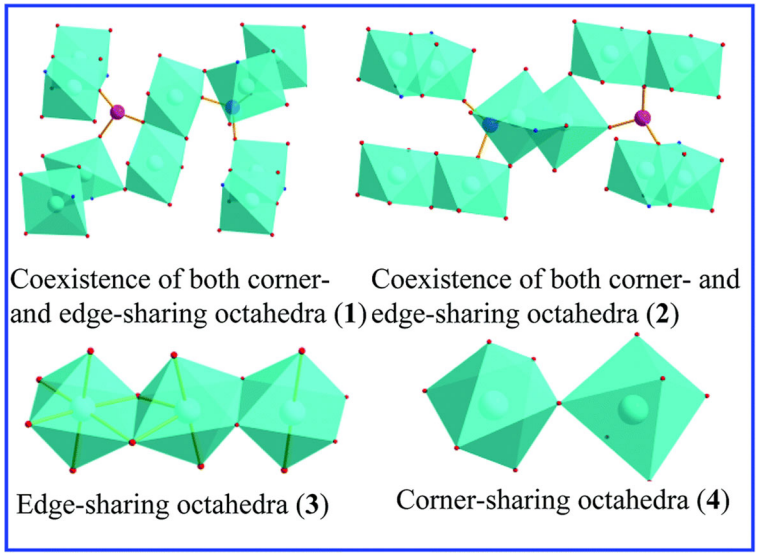

Fig. 9 Polyhedral models of corner- and edge-sharing octahedral cobalt in 1–4. All metal centers are octahedrally coordinated. Co, O, P, and N are shown as cyan, red, magenta, blue, respectively. Reproduced with permission (Zhou et al. 2015). Copyright 2015, Royal Society of Chemistry

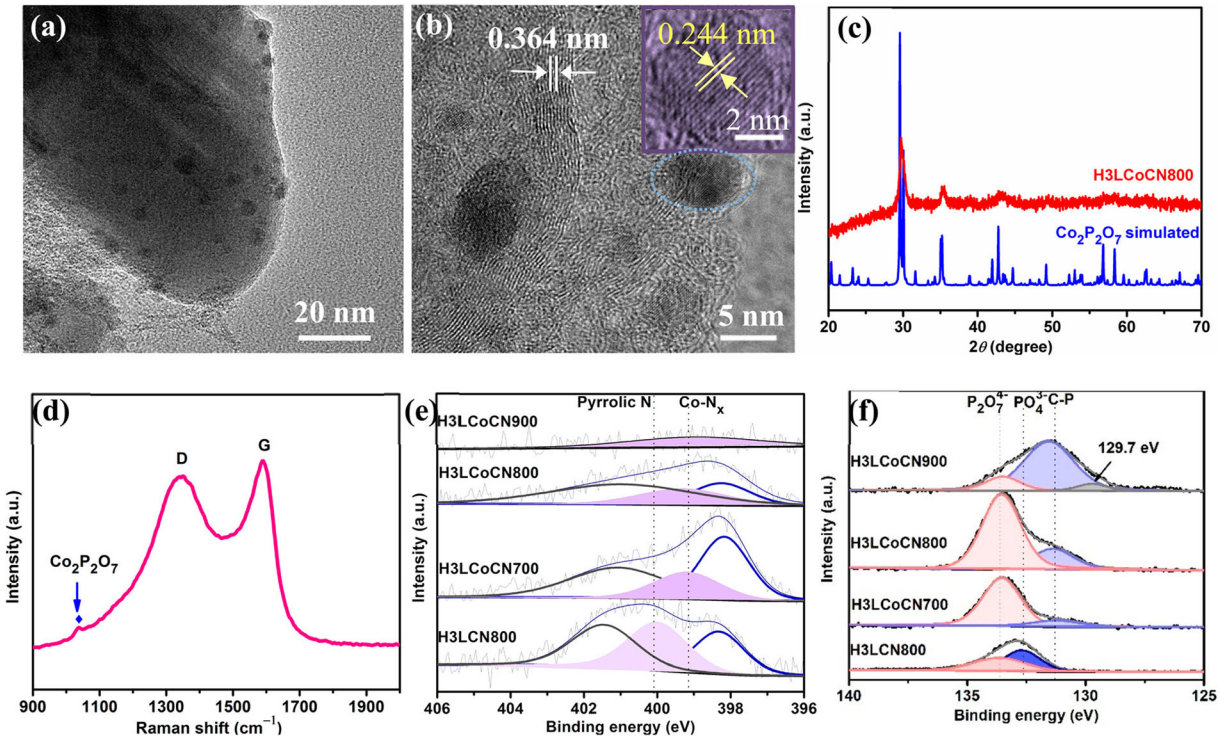

Fig. 10 Characterization of H3LCoCN800. **a** TEM image. **b** HRTEM image (Inset: an individual nanoparticle). **c** XRD patterns. **d** Raman spectrum. High-resolution XPS spectra of N 1 s (**e**), and P 2p (**f**). Reproduced with permission (Zhou et al. 2017). Copyright 2017, American Chemical Society

geometry, with longer Co-O and Co-Co distances, compared to those in $Co_3(PO_4)_2$, which has been suggested to favor water adsorption and lower the activation barrier of O-O bond formation. TEM and XANES analysis of the material after catalysis revealed the formation of a thin amorphous film with thickness of ca. 1 nm on the surface of the catalyst. The contribution of the doped carbon surrounding the cobalt phosphate species to the activity was evaluated by measuring the activity of N-free catalyst. The N-free catalyst displayed the identical OER onset potential and overpotential at j = 10 mA cm^{-2} as the N-containing catalyst, but the latter exhibited higher current density at an overpotential of 300 mV.

Conclusion and outlook

Metal phosphonates are a family of coordination polymers in which metals are coordinated to organophosphonate ligands. Phosphonate ligands form relatively strong bonds with most metals and generally, simple monophosphonates tend to produce layered structures. Nevertheless, several strategies have been developed over the last decades for producing porous compounds. In comparison with other hybrid materials, metal phosphonates have high thermal and chemical stabilities, finding application in many fields including catalysis, adsorption, gas storage, biotechnology, and sensing. Recently, they have shown promise for energy storage and conversion.

Herein, we have reviewed the utilization of metal phosphonates as precursors for HER and OER electrocatalysts. Phosphonates are valuable precursors for metal phosphide HER electrocatalysts, allowing the synthesis of phosphides through calcination procedures under inert atmosphere, in certain conditions even without the need of further phosphorous sources or phosphorization steps. $Ni_{12}P_5$, Ni_2P, Co_2P/CoP nanoparticles coated with thin carbon films have been synthesized by calcination of layered phenylphosphonates, whereas CoP or Cu_3P NPs loaded on porous P,N-codoped carbon networks have been fabricated from phosphonate-based MOFs with an additional N-containing ligand. These strategies have led to active metal phosphide electrocatalysts for the HER in acidic

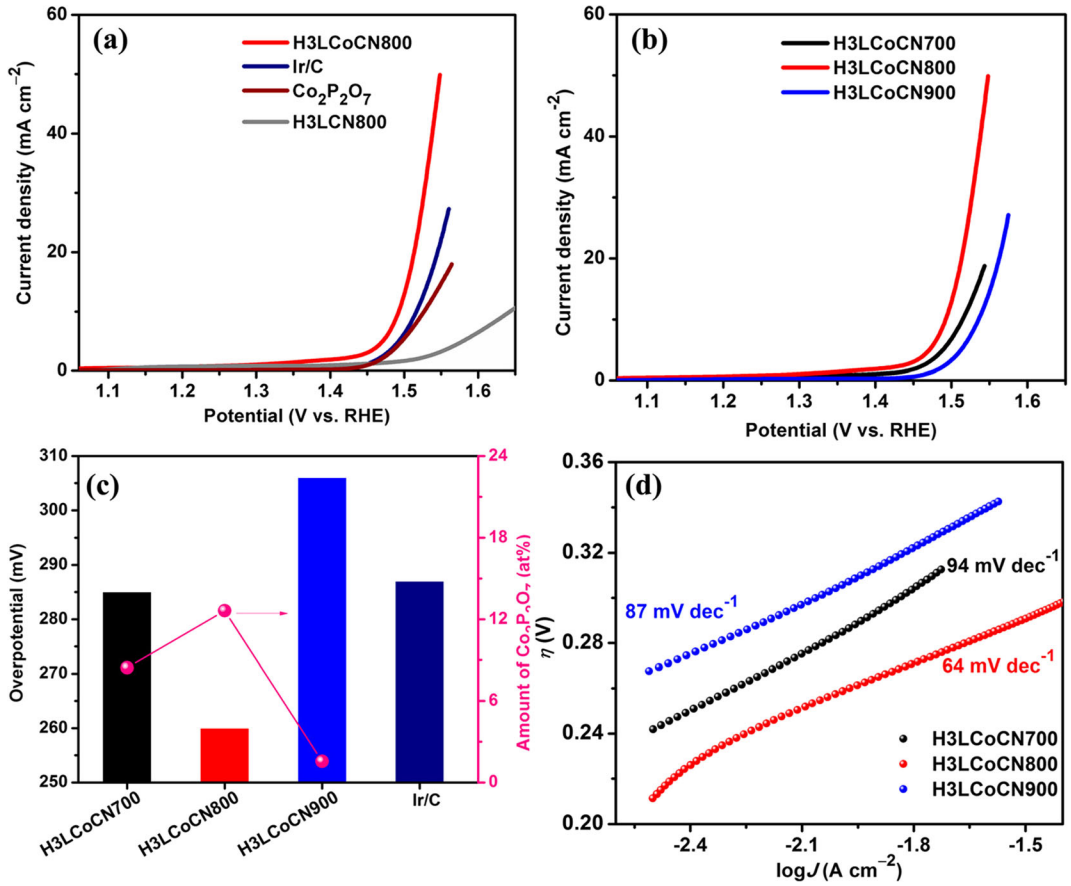

Fig. 11 **a** IR-corrected LSV curves of H3LCoCN800, metal-free H3LCN800, Ir/C, and $Co_2P_2O_7$ on glassy carbon (GC) electrode at a scan rate of 5 mV s^{-1}. **b** IR-corrected LSV curves of H3LCoCNX obtained at different pyrolysis temperatures at a scan rate of 5 mV s^{-1}. **c** The relationship between the amount of $Co_2P_2O_7$ and OER activity in terms of overpotential at 10 mA cm^{-2}. **d** Tafel slope of H3LCoCNX. All tests were performed in 1.0 M KOH media. Loading: 0.41 mg/cm^2. Reproduced with permission (Zhou et al. 2017). Copyright 2017, American Chemical Society

media, as well as to catalysts more resistant against dissolution at low pH owing to the protective effect of the carbon coatings.

Metal phosphonates have also been successfully explored as ex situ and in situ precursors for OER electrocatalysts, or utilized directly as water oxidation catalysts. A highly active cobalt phosphate NPs/N-doped carbon nanocomposite has been synthesized by calcination of a layered cobalt phosphonate. Layered and porous metal phosphonates act as in situ precursors for oxyhydroxides OER catalysts in alkaline medium. They seem to act also as in situ templates for the morphology of the active catalyst and possibly also for the local structure of the metal active sites, although further work is required to understand and explore these aspects. A series of layered cobalt phosphonates with well-defined crystal structures were investigated as water oxidation catalysts, allowing to establish correlations between the activity observed and specific structural features of the materials. These types of studies provide valuable information for the future design of water oxidation catalysts.

Until now, research has been centered mainly on single metal phosphonates, mostly on cobalt phosphonates, and on a limited number of ligands. Future work on the use of phosphonates as precursors for phosphides, phosphates, and in situ precursors should extend the range of metals, and also combinations of metals for exploring synergies. The influence of the morphology, metal local structures, and surface area of the metal phosphonates acting as in situ precursors/templates on the activity needs to be further investigated. The high chemical stability and low solubilities of phosphonates containing high valence metals are

attractive characteristics for designing hybrid phosphonate compounds that are the active catalyst. This is however very challenging, as the materials need to combine stability with very active catalytic sites and appropriate electroconductivity.

Funding information R.Z. acknowledges the fellowship from the China Scholarship Council (CSC). P.A.R. acknowledges the support from the DFG (RU2012/2-1).

Compliance with ethical standards

Conflict of interest The authors declare that they have no conflict of interest.

References

Alberti G, Vivani R, Marmottini F, Zappelli P (1998) Microporous solids based on pillared metal(IV) phosphates and phosphonates. J Porous Mater 5:205–220. https://doi.org/10.1023/a:1009678120336

Bai Y, Zhang H, Li X, Liu L, Xu H, Qiu H, Wang Y (2015) Novel peapod-like Ni_2P nanoparticles with improved electrochemical properties for hydrogen evolution and lithium storage. Nanoscale 7:1446–1453. https://doi.org/10.1039/C4NR05862C

Chen W-F, Sasaki K, Ma C, Frenkel AI, Marinkovic N, Muckerman JT, Zhu Y, Adzic RR (2012) Hydrogen-evolution catalysts based on non-noble metal nickel–molybdenum nitride Nanosheets. Angew Chem Int Ed 51:6131–6135. https://doi.org/10.1002/anie.201200699

Chen X, Peng Y, Han X, Liu Y, Lin X, Cui Y (2017) Sixteen isostructural phosphonate metal-organic frameworks with controlled Lewis acidity and chemical stability for asymmetric catalysis. Nat Commun 8:2171. https://doi.org/10.1038/s41467-017-02335-0

Cheng L, Huang W, Gong Q, Liu C, Liu Z, Li Y, Dai H (2014) Ultrathin WS_2 nanoflakes as a high-performance electrocatalyst for the hydrogen evolution reaction. Angew Chem Int Ed 53:7860–7863. https://doi.org/10.1002/anie.201402315

Clearfield A (1998a) Organically pillared micro- and mesoporous materials. Chem Mater 10:2801–2810. https://doi.org/10.1021/cm9802191

Clearfield A (1998b) Metal phosphonate chemistry. In: Karlin KD (Ed) Progress in inorganic chemistry, vol. 47. John Wiley & Sons, Inc., New York, pp 371–510. https://doi.org/10.1002/9780470166482.ch4

Clearfield A, Demandis K (eds) (2011) Metal phosphonate chemistry: from synthesis to applications RSC publishing. UK. https://doi.org/10.1039/9781849733571

Cook TR, Dogutan DK, Reece SY, Surendranath Y, Teets TS, Nocera DG (2010) Solar energy supply and storage for the legacy and nonlegacy worlds. Chem Rev 110:6474–6502. https://doi.org/10.1021/cr100246c

Dau H, Limberg C, Reier T, Risch M, Roggan S, Strasser P (2010) The mechanism of water oxidation: from electrolysis via homogeneous to biological catalysis. ChemCatChem 2:724–761. https://doi.org/10.1002/cctc.201000126

Dines MB, Cooksey RE, Griffith PC, Lane RH (1983) Mixed-component layered tetravalent metal phosphonates/phosphates as precursors for microporous materials. Inorg Chem 22:1003–1004. https://doi.org/10.1021/ic00148a036

Downes CA, Marinescu SC (2017) Electrocatalytic metal–organic frameworks for energy applications. ChemSusChem 10:4374–4392. https://doi.org/10.1002/cssc.201701420

El Haskouri J, Guillem C, Latorre J, Beltrán A, Beltrán D, Amorós P (2004) S+I- ionic formation mechanism to new mesoporous aluminum phosphonates and diphosphonates. Chem Mater 16:4359–4372. https://doi.org/10.1021/cm048988+

Gagnon KJ, Perry HP, Clearfield A (2012) Conventional and unconventional metal–organic frameworks based on phosphonate ligands: MOFs and UMOFs. Chem Rev 112:1034–1054. https://doi.org/10.1021/cr2002257

Gong M, Li Y, Wang H, Liang Y, Wu JZ, Zhou J, Wang J, Regier T, Wei F, Dai H (2013) An advanced Ni–Fe layered double hydroxide electrocatalyst for water oxidation. J Am Chem Soc 135:8452–8455. https://doi.org/10.1021/ja4027715

Goura J, Chandrasekhar V (2015) Molecular metal phosphonates. Chem Rev 115:6854–6965. https://doi.org/10.1021/acs.chemrev.5b00107

Gray HB (2009) Powering the planet with solar fuel. Nat Chem 1:7. https://doi.org/10.1038/nchem.141

Han L, Dong S, Wang E (2016) Transition-metal (Co, Ni, and Fe)-based electrocatalysts for the water oxidation reaction. Adv Mater 28:9266–9291. https://doi.org/10.1002/adma.201602270

Hunter BM, Gray HB, Müller AM (2016) Earth-abundant heterogeneous water oxidation catalysts. Chem Rev 116:14120–14136. https://doi.org/10.1021/acs.chemrev.6b00398

Kanan MW, Nocera DG (2008) In situ formation of an oxygen-evolving catalyst in neutral water containing phosphate and Co^{2+}. Science 321:1072–1075. https://doi.org/10.1126/science.1162018

Kim H, Park J, Park I, Jin K, Jerng SE, Kim SH, Nam KT, Kang K (2015) Coordination tuning of cobalt phosphates towards efficient water oxidation catalyst. Nat Commun 6:8253. https://doi.org/10.1038/ncomms9253

Kong D, Wang H, Cha JJ, Pasta M, Koski KJ, Yao J, Cui Y (2013) Synthesis of MoS_2 and $MoSe_2$ films with vertically aligned layers. Nano Lett 13:1341–1347. https://doi.org/10.1021/nl400258t

Lewis NS, Nocera DG (2006) Powering the planet: chemical challenges in solar energy utilization. Proc Natl Acad Sci U S A 103:15729–15735. https://doi.org/10.1073/pnas.0603395103

Liu Y, Guo S-X, Bond AM, Zhang J, Du S (2013) Cobalt(II) phosphonate coordination polymers: synthesis, characterization and application as oxygen evolution electrocatalysts in aqueous media and water-saturated hydrophobic 1-butyl-3-methylimidazolium hexafluorophosphate ionic liquid. Electrochim Acta 101:201–208. https://doi.org/10.1016/j.electacta.2012.09.093

Ma T-Y, Yuan Z-Y (2010) Organic-additive-assisted synthesis of hierarchically meso-/macroporous titanium phosphonates.

Eur J Inorg Chem 2010:2941–2948. https://doi.org/10.1002/ejic.201000204

Ma T-Y, Yuan Z-Y (2011) Metal phosphonate hybrid mesostructures: environmentally friendly multifunctional materials for clean energy and other applications. ChemSusChem 4:1407–1419. https://doi.org/10.1002/cssc.201100050

Ma T-Y, Lin X-Z, Yuan Z-Y (2010) Cubic mesoporous titanium phosphonates with multifunctionality. Chem Eur J 16:8487–8494. https://doi.org/10.1002/chem.201000364

Maeda K (2004) Metal phosphonate open-framework materials. Microporous Mesoporous Mater 73:47–55. https://doi.org/10.1016/j.micromeso.2003.10.018

McCrory CCL, Jung S, Ferrer IM, Chatman SM, Peters JC, Jaramillo TF (2015) Benchmarking hydrogen evolving reaction and oxygen evolving reaction electrocatalysts for solar water splitting devices. J Am Chem Soc 137:4347–4357. https://doi.org/10.1021/ja510442p

McKone JR, Sadtler BF, Werlang CA, Lewis NS, Gray HB (2013) Ni–Mo Nanopowders for efficient electrochemical hydrogen evolution. ACS Catal 3:166–169. https://doi.org/10.1021/cs300691m

Mei P, Pramanik M, Lee J, Ide Y, Alothman ZA, Kim JH, Yamauchi Y (2017) Highly ordered mesostructured vanadium phosphonate toward electrode materials for lithium-ion batteries. Chem Eur J 23:4344–4352. https://doi.org/10.1002/chem.201604159

Morozan A, Jaouen F (2012) Metal organic frameworks for electrochemical applications energy environ. Sci 5:9269–9290. https://doi.org/10.1039/C2EE22989G

Mutin PH, Guerrero G, Alauzun JG (2015) Sol-gel processing of phosphonate-based organic-inorganic hybrid materials. J Ceramic Soc Jpn 123:709–713. https://doi.org/10.2109/jcersj2.123.709

Pan Y, Hu W, Liu D, Liu Y, Liu C (2015) Carbon nanotubes decorated with nickel phosphide nanoparticles as efficient nanohybrid electrocatalysts for the hydrogen evolution reaction. J Mater Chem A 3:13087–13094. https://doi.org/10.1039/C5TA02128F

Polarz S, Smarsly B, Bronstein L, Antonietti M (2001) From cyclodextrin assemblies to porous materials by silica templating. Angew Chem Int Ed 40:4417–4421. https://doi.org/10.1002/1521-3773(20011203)40:23<4417::AID-ANIE4417>3.0.CO;2-P

Poojary DM, Grohol D, Clearfield A (1995) Synthesis and X-ray powder structure of a novel porous uranyl phenylphosphonate containing unidimensional channels flanked by hydrophobic regions. Angew Chem Int Ed 34:1508–1510. https://doi.org/10.1002/anie.199515081

Popczun EJ, McKone JR, Read CG, Biacchi AJ, Wiltrout AM, Lewis NS, Schaak RE (2013) Nanostructured nickel phosphide as an electrocatalyst for the hydrogen evolution reaction. J Am Chem Soc 135:9267–9270. https://doi.org/10.1021/ja403440e

Pramanik M, Tsujimoto Y, Malgras V, Dou SX, Kim JH, Yamauchi Y (2015) Mesoporous iron phosphonate electrodes with crystalline frameworks for lithium-ion batteries. Chem Mater, 27:1082–1089. https://doi.org/10.1021/cm5044045

Reier T, Nong HN, Teschner D, Schlögl R, Strasser P (2017) Electrocatalytic oxygen evolution reaction in acidic environments – reaction mechanisms and catalysts. Adv. Energy Mater 7:1601275. https://doi.org/10.1002/aenm.201601275

Risch M, Shevchenko D, Anderlund MF, Styring S, Heidkamp J, Lange KM, Thapper A, Zaharieva I (2012) Atomic structure of cobalt-oxide nanoparticles active in light-driven catalysis of water oxidation. Int J Hydrogen Energy 37:8878–8888. https://doi.org/10.1016/j.ijhydene.2012.01.138

Saha J, Chowdhury DR, Jash P, Paul A (2017) Cobalt phosphonates as precatalysts for water oxidation: role of pore size in catalysis. Chem Eur J 23:12519–12526. https://doi.org/10.1002/chem.201700882

Salunkhe RR, Kaneti YV, Yamauchi Y (2017) Metal–organic framework-derived nanoporous metal oxides toward supercapacitor applications: progress and prospects. ACS Nano 11:5293–5308. https://doi.org/10.1021/acsnano.7b02796

Shevchenko D, Anderlund MF, Thapper A, Styring S (2011) Photochemical water oxidation with visible light using a cobalt containing catalyst. Energy Environ Sci 4:1284–1287. https://doi.org/10.1039/C0EE00585A

Shimizu GKH, Vaidhyanathan R, Taylor JM (2009) Phosphonate and sulfonate metal organic frameworks. Chem Soc Rev 38:1430–1449. https://doi.org/10.1039/B802423P

Stern L-A, Feng L, Song F, Hu X (2015) Ni_2P as a Janus catalyst for water splitting: the oxygen evolution activity of Ni_2P nanoparticles. Energy Environ Sci 8:2347–2351. https://doi.org/10.1039/C5EE01155H

Stevens MB, Enman LJ, Batchellor AS, Cosby MR, Vise AE, Trang CDM, Boettcher SW (2017) Measurement techniques for the study of thin film heterogeneous water oxidation electrocatalysts. Chem Mater 29:120–140. https://doi.org/10.1021/acs.chemmater.6b02796

Suen N-T, Hung S-F, Quan Q, Zhang N, Xu Y-J, Chen HM (2017) Electrocatalysis for the oxygen evolution reaction: recent development and future perspectives. Chem Soc Rev 46:337–365. https://doi.org/10.1039/C6CS00328A

Trotochaud L, Ranney JK, Williams KN, Boettcher SW (2012) Solution-cast metal oxide thin film electrocatalysts for oxygen evolution. J Am Chem Soc 134:17253–17261. https://doi.org/10.1021/ja307507a

Turner JA (2004) Sustainable hydrogen production. Science 305:972–974. https://doi.org/10.1126/science.1103197

Vrubel H, Hu X (2012) Molybdenum boride and carbide catalyze hydrogen evolution in both acidic and basic solutions. Angew Chem Int Ed 51:12703–12706. https://doi.org/10.1002/anie.201207111

Wang R, Dong XY, Du J, Zhao JY, Zang SQ (2017) MOF-derived bifunctional Cu3P nanoparticles coated by a N,P-codoped carbon shell for hydrogen evolution and oxygen reduction. Adv Mater 30. https://doi.org/10.1002/adma.201703711

Wang R, Dong X-Y, Du J, Zhao J-Y, Zang S-Q MOF-derived bifunctional Cu3P nanoparticles coated by a N,P-codoped carbon shell for hydrogen evolution and oxygen reduction. Adv Mater 1703711 doi:https://doi.org/10.1002/adma.201703711, 2018

Wharmby MT, Miller SR, Groves JA, Margiolaki I, Ashbrook SE, Wright PA (2010) Yttrium bisphosphonate STA-13: a racemic phosphonate metal organic framework with permanent microporosity. Dalton Trans 39:6389–6391. https://doi.org/10.1039/C0DT00233J

Xiao P, Chen W, Wang X (2015) A review of phosphide-based materials for electrocatalytic hydrogen evolution. Adv Energy Mater 5:1500985. https://doi.org/10.1002/aenm.201500985

Xing Z, Liu Q, Asiri AM, Sun X (2014) Closely interconnected network of molybdenum phosphide nanoparticles: a highly efficient electrocatalyst for generating hydrogen from water. Adv Mater 26:5702–5707. https://doi.org/10.1002/adma.201401692

Zeng M, Li Y (2015) Recent advances in heterogeneous electrocatalysts for the hydrogen evolution reaction. J Mater Chem A 3:14942–14962. https://doi.org/10.1039/C5TA02974K

Zhang R, Russo PA, Buzanich AG, Jeon T, Pinna N (2017a) Hybrid organic–inorganic transition-metal phosphonates as precursors for water oxidation electrocatalysts. Adv Funct Mater 27:1703158. https://doi.org/10.1002/adfm.201703158

Zhang R, Russo PA, Buzanich AG, Jeon T, Pinna N (2017b) Hybrid organic–inorganic transition-metal phosphonates as precursors for water oxidation electrocatalysts. Adv Funct Mater 27. https://doi.org/10.1002/adfm.201703158

Zhang R, Russo PA, Feist M, Amsalem P, Koch N, Pinna N (2017c) Synthesis of nickel phosphide electrocatalysts from hybrid metal phosphonates. ACS Appl Mater Interfaces 9:14013–14022. https://doi.org/10.1021/acsami.7b01178

Zhou T, Wang D, Chun-Kiat Goh S, Hong J, Han J, Mao J, Xu R (2015) Bio-inspired organic cobalt(ii) phosphonates toward water oxidation. Energy Environ Sci 8:526–534. https://doi.org/10.1039/C4EE03234A

Zhou T, du Y, Wang D, Yin S, Tu W, Chen Z, Borgna A, Xu R (2017) Phosphonate-based metal–organic framework derived co–P–C hybrid as an efficient electrocatalyst for oxygen evolution reaction. ACS Catal 7:6000–6007. https://doi.org/10.1021/acscatal.7b00937

Zhu J, Bu X, Feng P, Stucky GD (2000) An open-framework material with dangling organic functional groups in 24-ring channels. J Am Chem Soc 122:11563–11564. https://doi.org/10.1021/ja002118l

Zhu Y-P, Ma T-Y, Liu Y-L, Ren T-Z, Yuan Z-Y (2014) Metal phosphonate hybrid materials: from densely layered to hierarchically nanoporous structures. Inorg Chem Front 1:360–383. https://doi.org/10.1039/C4QI00011K

Zhu Y-P, Ren T-Z, Yuan Z-Y (2015a) Insights into mesoporous metal phosphonate hybrid materials for catalysis. Cat Sci Technol 5:4258–4279. https://doi.org/10.1039/C5CY00107B

Zhu Y-P, Xu X, Su H, Liu Y-P, Chen T, Yuan Z-Y (2015b) Ultrafine metal phosphide nanocrystals in situ decorated on highly porous heteroatom-doped carbons for active electrocatalytic hydrogen evolution. ACS Appl Mater Interfaces 7:28369–28376. https://doi.org/10.1021/acsami.5b09092